
White Rose Research Online

eprints@whiterose.ac.uk
https://eprints.whiterose.ac.uk
Universities of Leeds, Sheffield and York

Deposited via The University of Leeds.

White Rose Research Online URL for this paper:
https://eprints.whiterose.ac.uk/id/eprint/167368/

Version: Accepted Version

Article:
Allulakshmi, K, Vinod, JS, Heitor, A et al. (2021) DEM Study on the Instability Behaviour of Granular Materials. Geotechnical and Geological Engineering, 39. pp. 2175-2185. ISSN: 0960-3182

https://doi.org/10.1007/s10706-020-01617-7

© Springer Nature Switzerland AG 2020. This is an author produced version of a journal article published in Geotechnical and Geological Engineering. Uploaded in accordance with the publisher's self-archiving policy.

Reuse
Items deposited in White Rose Research Online are protected by copyright, with all rights reserved unless indicated otherwise. They may be downloaded and/or printed for private study, or other acts as permitted by national copyright laws. The publisher or other rights holders may allow further reproduction and re-use of the full text version. This is indicated by the licence information on the White Rose Research Online record for the item.

Takedown
If you consider content in White Rose Research Online to be in breach of UK law, please notify us by emailing eprints@whiterose.ac.uk including the URL of the record and the reason for the withdrawal request.

UNIVERSITY OF LEEDS

University of Sheffield

UNIVERSITY of York

DEM Study on the Instability Behaviour of Granular Materials

Krishna Allulakshmi[1], Jayan S. Vinod[1*], Ana Heitor[2], Andy Fourie[3], David Reid[3]

[1]Faculty of Engineering and Information Sciences, University of Wollongong, NSW 2522, Australia.

[2]Faculty of Engineering and Physical Sciences, University of Leeds, Leeds LS@ 9DY,UK

[3]Faculty of Engineering and Mathematical Sciences, University of Western Australia, WA 6009, Australia.

*Corresponding author (Email: vinod@uow.edu.au)

Abstract

This paper presents the Discrete Element Method (DEM) simulations on the instability behaviour of granular materials during Constant Shear Drained condition (CSD). CSD condition was implemented by decreasing mean effective stress on an assembly of particles under strain controlled loading. In this study, the instability condition was predicted at the particle scale level using particle second order work increment (Nicot et al., 2012). The DEM contact parameters have been calibrated to capture the macroscopic responses and the instability behaviour consistently with the laboratory experimental observations. Using the same contact parameters the effect of different range of initial states at the beginning of CSD condition such as different initial mean effective stress (p_0'), void ratio (e_0) and deviatoric stress (q) on the instability behaviour were analysed. In addition, the micromechanical parameters such as coordination number, anisotropic coefficients (geometric, mechanical) have been extracted to assist in characterising the instability behaviour during CSD condition. The initial stress state of the soil (i.e. at the onset of CSD) condition has shown a significant influence on the evolution of anisotropic coefficients, an evident behaviour change was noted once the CSD condition is imposed. A continuous increase of geometric anisotropy, and a gradual decrease of mechanical anisotropy was observed after the instability condition is reached.

Keywords: discrete element method, constant shear stress, particle scale instability, anisotropy.

Introduction

Water ingress in soils through infiltration can trigger instability leading to failures in slopes and embankments under drained conditions. Subsequent investigations on such failures have shown that the infiltration of water in soils can cause a reduction in effective stress leading to the instability of slopes and embankments (e.g. Eckersley 1990; Olson et al. 2000; Dong et al. 2015; Lashkari et al. 2019). Brand (1981) and Sasitharan et al. (1993) have suggested constant shear drained (CSD) triaxial test to predict the instability caused by the reduction in effective stress. In the recent past, several researchers have conducted CSD laboratory tests to investigate the instability behaviour of different soils (e.g. Skopek et al. 1994, Anderson and Riemer 1995; Zhu and Anderson 1998; Gajo et al. 2000; Chu et al. 2003, 2012; Nicot et al. 2011; Dong et al. 2015; Rabbi et al. 2019).

Instability in CSD tests indicates the sudden development of large plastic strains correlated with the inability of the soil to sustain the imposed load (Skopek et al. 1994; Chu et al. 2003; Sawicki and Swidzinski 2010; Dong et al. 2015). Hill (1958) proposed the instability criterion in terms of second order work as a function of stress-strain ($d^2W = d\sigma' d\varepsilon$) has been widely used to identify the instability behaviour during CSD conditions (e.g. Darve et al. 2004, 2007; Sibille et al. 2007; Daouadji et al. 2010; Nicot et al. 2011; Dong et al. 2015). Based on Hill's criterion, the material is stable if the second increment of work is strictly positive ($d^2W > 0$) for all changes in stresses and strains (Darve et al. 2004). In addition, many constitutive models have also incorporated Hill's instability criterion to capture the instability during CSD tests (Ramos et al. 2012; Alipour and Lashkari 2017; Lashkari et al. 2019). Recently, Nicot et al. (2012) have proposed a microscopic formulation for the second order work as a combination of contact forces and resultant particle forces. This approach enables the identification of the instability point at the particle scale level and provides more insight to address the instability from the micromechanical perspective with the local governing variables (Hadda et al. 2013).

The Discrete Element Method (DEM) developed by Cundall and Strack (1979) is an alternative to the continuum mechanics approach for modelling and analysing the soil mechanical behaviour at a particle scale level. Even though many experimental CSD analyses have been conducted on the instability of granular materials, only, limited studies were performed to simulate the CSD test using micromechanical based approaches such as DEM (Ning et al. 2013; Perez et al. 2016; Lashkari et al. 2019). Perez et al. (2016) and Lashkari et al. (2019) have adopted a stress controlled loading in their analyses and identified the instability behaviour

based on Hill's particle scale criterion and strain rate increment. Furthermore, they simulated the evolution of micromechanical quantities (coordination number, anisotropic coefficients) and highlighted the behavioural change of micro parameters post the instability point.

It is evident from the literature that all the DEM studies on CSD had adopted a stress controlled loading condition. However, in this study, CSD condition was simulated under strain controlled loading and performed a detailed micromechanical analysis of soil specimen under constant shear load. The effect of different type of initial stress state at the beginning of the CSD condition (i.e. q, p', e_0) on the onset of instability condition has been studied. The macroscopic responses obtained from the numerical results (in the $q - p'$ space) are compared with the experimental investigations reported by Dong et al. (2015) on Toyoura sand. In addition, the instability behaviour at the particle scale level, has been identified using Nicot et al. (2012) second order work increment. Furthermore, the response of micromechanical parameters (e.g. coordination number, anisotropic coefficients) and their evolution under these controlled loading conditions has been investigated.

Numerical simulation program

A cylindrical specimen having 33,480 spherical particles (see Fig.1 (b)) was created to mimic the particle size distribution shown in Figure 1 (a). A non-linear Hertz-Mindlin (H-M) contact model was used to capture all the particle interactions. The elastic particles in three-dimensional assemblies are expected to interact in a non-linear fashion, a non-linear contact model is considered as a simple contact model for soils and often used in many DEM simulations to capture the characteristic behaviour of soil (e.g. Cui and O'Sullivan 2006; Sitharam et al. 2008; O'Sullivan 2011). The Hertz-Mindlin (H-M) contact model, used in these simulations is derived by considering the interaction of two elastic particles, and the particle stiffness values are determined using material properties**.** The material properties are particle shear modulus of 12 GPa, particle Poisson's ratio of 0.15, contact friction value of 0.3, particle density of 2650 kg/m^3, local damping coefficient of 0.1, gravity was zero in these simulations. All simulations were carried out using PFC3D code (Itasca 2016).

After generating particles in the cylindrical chamber, the assembly was brought to an equilibrium state before applying any loading. Then, the system was subjected to isotropic compression up to a desired initial mean effective stress (p_0'). During the consolidation stage, the specimen was loaded in a strain-controlled manner, with constant velocities imposed on the boundary walls using a servo-control mechanism until a target confining stress was achieved

(Itasca 2016). The void ratio obtained at the end of isotropic compression was (e_0 = 0.562). After reaching the initial stress state, the specimens were sheared under drained conditions to specific deviatoric stresses (q) of 120, 150 and 180 kPa. Then a CSD stress path was implemented in the same manner as suggested by (Ning et al. 2013), where the mean effective stress was decreased gradually, this procedure enables a constant shear load (constant (q) path) throughout a CSD test. The strain rate used in the current study was of strain 0.005 s^{-1}. As the loading conditions are strain controlled it is always ensured that the system is in quasi-static regime by monitoring the inertial number $I = \dot{\varepsilon} d\sqrt{\rho/p'}$ in which p′ is mean effective stress, d is mean particle size, ρ is particle density and $\dot{\varepsilon}$ is strain rate (MiDi 2004). Based on the simulation configuration considered in this work, the inertial number was calculated, and it was less than ($I < 3 \times 10^{-3}$), thereby ensuring all the simulations presented in the current study are under quasi-static loading conditions. The stress ratio ($\eta = q/p'$) at the onset of CSD was (η_{CSD} = 0.5, 0.59 and 0.69). In this study, the stresses within the assembly were calculated using Eq. 1 (Bagi 1996).

$$\sigma_{ij} = \frac{1}{V} \sum_{1}^{N_c} f_i l_j \tag{1}$$

where, σ_{ij} is the stress tensor, V is the volume of the cylindrical chamber, l_j is the jth component of the branch vector l that joins the centres of two particles in contact, f_i is the ith component of the contact force vector f, and N_c is the total number of contacts in the domain.

In this study, the rigid-wall boundary condition was adopted for all the simulations, and the boundary effect arises due to this condition was minimised by following certain specific criteria's (e.g. maintaining a high ratio of sample diameter to maximum particle size, calculation of stress responses internally with particle-particle contacts), as mentioned in the literature (e.g. Head 1994; Marketos and Bolton 2010; Fu and Dafalias 2011; Huang et al. 2014). Head (1994) suggested that the ratio of sample diameter to maximum particle size should be higher than 10. This criteria was adopted in this study, where at the end of consolidation stage the ratio was 10. Moreover, to avoid the rigid-boundary constrain, the stress responses have been measured internally with particle-particle contacts using Eq. (1) rather than at the boundaries. In addition, the deviatoric fabric ($\emptyset_d$) is the difference of maximum and minimum eigenvalues was calculated using fabric tensor of contact normals defined by Satake (1982). The ($\emptyset_d$) value at the beginning of the shearing stage was of 0.004, ensuring an isotropic packing of the sample, amidst rigid boundaries.

Calibration of the model with laboratory experimental data

For the reference purpose, recent experimental investigations of Dong et al. (2015) on loose Toyoura sand subjected to CSD loading conditions are considered here, and the DEM model has been calibrated to the laboratory results reported in Dong et al. (2015). The material parameters mentioned in the above section were calibrated properties. Simulation results of three CSD tests, along with experimental results, are shown in Figure 2. Here 'diamond' markers indicate the onset of CSD loading, whereas 'cross' markers relate to the onset of instability. The same notation is followed in all the following figures. It is to be noted that diffuse failure mode under constant shear loading and the associated instability behaviour is considered in this study.

It is evident from Figure 2 that the DEM model has captured the CSD test qualitatively compared to the experimental results. After instability, the specimen shows a gradual decrease of q, indicating the inability to withstand the imposed constant deviatoric stress. The stress ratio at instability (η_{IL}) predicted from the DEM model using Nicot et al. (2012) particle scale second order work is in the range of (η_{IL} = 0.7 – 0.75), which is in good agreement with the experimental-instability of (η_{IL} = 0.72 – 0.74) (Dong et al. 2015).

Instability point using particle scale second order work proposed by Nicot et al. (2012)

Many studies (e.g. Darve et al. 2004, 2007; Daouadji et al. 2010; Nicot et al. 2011; Dong et al. 2015; Rabbi et al. 2019) have successfully identified the instability point using Hill (1958) second order work criterion in CSD tests. However, in this study, the instability points were identified at the particle scale from the 'sign change of second order work' (occurrence of negative values in W_2^P) proposed by Nicot et al. (2012) given in Eq. 2.

$$W_2^P = \sum_{c \forall V} \delta f_i^c \delta l_i^c + \sum_{p \forall V} \delta f_i^p \delta x_i^p \quad (2)$$

Where, l^c is the branch vector joins the centres of two particles in contact, f^c the inter-particle contact force, x^p the position of particle 'p' and , f^p the resultant force applied for the particle 'p'.

It captures the changes in contact force and resultant forces acting on particles and can, therefore, provide more insight into the instability at the particle scale level. The results of three CSD simulations at stress ratios (η_{CSD} = 0.5, 0.59 and 0.69) predicting second order work, deviatoric stress and the ratio of incremental stress ratio dq/dp' versus time are plotted in

Figures 3 (a), (b), (c) respectively. The deviatoric stress response shows that the specimen is in a stable condition and can withstand the imposed constant deviatoric load. Later, the specimen shows the instability behaviour with the decrease in deviatoric stress, as it becomes difficult to sustain the imposed load. The instability behaviour can be understood as the inability of the particle assembly to withstand the continuously imposed static loads. The fluctuations (negative values) of particle scale second order work (W_2^P) represents the onset of instability within the particle assembly. The breakage of force chains along with the particles rearrangement post the onset of instability are the main contributing factors for the fluctuations in second order work. In addition, the incremental stress ratio (dq/dp') identifies the behavioural change in deviatoric stress throughout the test. The ratio was approximately zero until the instability point, after that as the sample experiences change in deviatoric stress, the dq/dp' ratio starts developing and increases gradually beyond the onset of instability. From Fig 3 (a), (b), (c), it can be observed that the negative values of W_2^P exactly coincides with the decline of deviatoric stress (q), the sudden increase in dq/dp' during the CSD shearing stage. The noticeable change in dq/dp', negative values of W_2^P, corresponding to the reduction in q occur concurrently and consistently with time for each stress ratio (η_{CSD}), indicating the onset of instability.

Effect of q on the instability point

Figure 4 (a), (b), (c) shows the macroscopic behaviour of the sample during CSD test of different stress ratios (η_{CSD} = 0.5, 0.59 and 0.69). The response of deviator stress (q), axial strain (ε_a) and void ratio (e) are plotted against mean effective stress p' respectively. It is evident from Figure 4 that (η_{CSD}) has a significant influence on the onset of instability. After the onset of CSD loading, q remains constant with a corresponding reduction of p'. However, once the reduction of p' reaches a particular value, q decreases gradually, highlighting that the sample cannot sustain the imposed constant q, thus indicating instability. From the axial strain behaviour, it can be noticed that after imposing CSD loading, the axial strain development was clearly influenced until the onset of instability. After that, the increase in axial strain rate has begun indicating instability, and axial strain has shown a steady increase with the corresponding decrease in p'. Similar response of ε_a against p' was also shown by Lashkari et al. (2019). Whereas, the e - p' plot shows an instant change in the behaviour once the CSD is imposed, the void ratio starts developing due to the rebound (relaxation) phenomena experienced by the soil with the decrease of mean effective stress under constant deviatoric

stress. And the void ratio response remains unaffected even after the onset of instability. Overall, regardless of the stress ratio at the onset of CSD, the void ratios and axial strains evolve in the same way.

Effect of p' on the instability behaviour

To investigate the effect of p' on the instability behaviour, two other different mean effective stress conditions are also considered (p'_0= 75, 500 kPa). Total three specimens were prepared by subjecting to different initial confining stresses of p'_0= 75, 200 and 500 kPa. And an initial void ratio of (e_0 = 0.56), was maintained for all three CSD simulations following isotropic compression. Before imposing CSD loading, the specimens were sheared to different deviatoric stress level in each test say for (p'_0= 75 kPa; q = 49 kPa), (p'_0= 200 kPa; q = 150 kPa) and (p'_0= 500 kPa; q = 240 kPa). From Fig 5 (a) it is inferred that regardless of initial p' and deviatoric stress applied prior to CSD loading, the soil undergoes instability and has got a unique instability line applicable during CSD loading. The instability line drawn from the origin connecting the instability points has a slope of (η_{IL} = 0.75). Similar observations of unique instability line in $q - p'$ plane for Hostun sand has been reported by Daouadji et al. (2010).

Figure 5 (b) shows the axial strain response against mean effective stress for p'_0= 75, 200, 500 kPa at q = 49,150, 240 kPa. In the case of high initial confining pressure (p'_0= 500 kPa and e_0 = 0.56), when the CSD loading is imposed, the specimen shows dilation behaviour, where the sample extends in the axial direction and reaches to 0.06 % from 0.065 % strain. After that, the specimen contracts and continues to show contraction behaviour throughout the test. A similar type of response in terms of reversal of ε_1 is consistent with the laboratory experimental findings reported by Nicot et al. (2011). Even though there is small dilation behaviour, no disturbance is observed in deviatoric stress response. The sample has sustained the imposed load by maintaining constant q (Fig 5(a)). This dilation tendency is only observed at high confining stresses. Whereas, the specimens at p'_0= 200 and 75 kPa show typical contraction behaviour in axial direction after the onset of CSD condition and remains the same throughout the test.

Effect of void ratio on the instability of granular materials

To investigate the influence of void ratio on the CSD instability subjected to similar loading conditions another particle assembly was created having a slightly higher void ratio of (e_0 = 0.585) at the end of the isotropic compression stage. The effect of void ratio in q - p' stress

plane is shown in Figure 6. It is evident that the instability point is significantly influenced by (e_0). For the q = 120 kPa condition, sample having (e_0 = 0.562) follows a longer stress path and shows a decrease in q at lower p' compared to the higher void ratio (e_0 = 0.585) specimen. Similarly, at a high magnitude of deviatoric stress (q = 180 kPa), q decreases instantly at the onset of CSD loading in the high void ratio (e_0 = 0.585) specimen indicating that the sample cannot withstand large magnitude constant q load. Similar behaviour of deviatoric stress for different void ratio samples during CSD loading was reported by Perez et al. (2016) and Lashkari et al. (2019).

Microscopic response during CSD shearing

The micromechanical behaviour of the granular assembly during a CSD stress path was captured with particle scale descriptors, namely average coordination number and structural anisotropy. The quantifying sources of structural anisotropy are geometrical anisotropy and mechanical anisotropy (Sitharam and Vinod 2010; Guo and Zhao 2013). Geometrical anisotropy is characterised based on the distribution of contact normals corresponding to the local orientation of the contact plane, while, mechanical anisotropy occurrence is due to contact forces which in turn are related to contact plane orientations (Iwashita and Oda 1999). The fabric tensor relation proposed by Satake (1982) is used in this study.

$$\emptyset_{ij} = \frac{1}{N_c}\sum_{1}^{N_c} n_i n_j \tag{3}$$

where, n_i is the unit contact normal and N_c is the total number of contacts. The deviatoric fabric $\emptyset_{ij}$ characterises the fabric anisotropy. It is reported that the stress ratio is the main element that can be associated for causing the overall anisotropic behaviour in a soil, (Rothenburg and Bathurst, 1989). The geometrical anisotropy, which is expressed based on the distribution of contact normals can also be termed as the contact anisotropy ($a_c = 15/2(\emptyset_1 - \emptyset_3)$), where $\emptyset_1$ and $\emptyset_3$ are the maximum and minimum eigenvalues of $\emptyset_{ij}$. The mechanical anisotropy which is dependent on the force vector can be distinguished into, normal force anisotropy a_n (due to normal contact forces) and tangential force anisotropy a_t (due to tangential contact forces). Perez et al. (2016) reported that the a_n, a_c anisotropic coefficients are more influenced by stress ratio under CSD loading. Hence these anisotropic coefficients have been emphasized in this study. Rothenburg and Bathurst (1989), Guo and Zhao (2013) defined normal force anisotropy a_n as follows:

$$F_{ij}^{n} = \frac{1}{4\pi}\int \bar{f}_n(V) n_i n_j dV$$

$$= \frac{1}{N_c}\sum_{1}^{N_c} \frac{f_n n_i n_j}{1 + (^{15}/_{2})\emptyset'_{kl} n_k n_l} \quad (4)$$

$$\bar{f}_n(V) = \overline{f^0}\left[1 + a_{ij}^{n}\right] \quad (5)$$

where, a_n is the second invariant of $a_{ij}^{n} = \left(^{15}/_{2}\right)\left(^{F_{ij}'^{n}}/_{\overline{f^0}}\right)$, here $\overline{f^0} = F_{ii}^{n}$ is the average normal contact force calculated over volume V, different from the mean normal contact force overall contacts.

The evolution of coordination numbers against time for three stress ratios (η_{CSD} = 0.5, 0.59 and 0.69) are illustrated in Figure 7 (a), (b) and (c) respectively The coordination number $Z = 2N_c/N_p$, where N_p, N_c are the number of particles and contacts, respectively. As shearing progresses, the coordination number begins to decrease continuously after the onset of CSD loading. As all the samples had the same initial void ratio (e_0), regardless of stress state (η) at the onset of CSD, the rate of decrease in coordination number remained uniform. The Z value at the instability point is approximately 4.8 irrespective of load (constant q) magnitude.

Figures 7 (a), (b) and (c) also presents the evolution of normal force anisotropy a_n, and contact anisotropy a_c against time for three stress ratios (η_{CSD} = 0.5, 0.59 and 0.69)respectively. It can be observed from figure 7 that the evolution of a_n is immediate upon shearing and increases linearly with time prior to CSD loading. After the onset of CSD, regardless of η, a nonlinear growth of a_n is observed, and its evolution clearly depends on deviatoric stress applied. After the instability point a_n reaches a peak value and then decreases gradually indicating the lack of ability to withstand the load while p' is decreasing.

However, the growth of a_c is different from a_n, where it is slow at the beginning until the onset of CSD, and the rate of increase in a_c is varied after CSD loading is imposed. The increase in a_c continues even after the instability point, which indicates that rearrangement of contacts in the loading direction to sustain the load (Perez et al. 2016; Lashkari et al. 2019). The continuous growth of a_c also suggests that fabric contacts are getting oriented in a more anisotropic way. The overall behaviour of a_c with time remained almost the same for all the stress states.

Comparison of stress ratio at instability with laboratory experimental data

The stress ratio and the corresponding void ratio at instability (e_{IL}) are plotted in Figure 8. The experimental data reported by Dong et al. (2015), Reid and Fourie (2019) are included for comparison. It is evident that the DEM simulations are able to predict the stress ratio at instability accurately and closely match the experimental results. This further strengthens the DEM model developed in this study as it could able to predict the instability of granular material during CSD loading qualitatively.

Conclusions

The results of the DEM simulations on the instability behaviour of granular materials during CSD testing conditions are reported in this paper. The particle-scale second order work relation, which was employed to identify the instability during CSD tests has captured the onset of instability, and it was consistent with the macroscopic behavioural change of deviatoric stress and axial strain. The axial strain shows steady growth and deviatoric stress decreases gradually post the instability point. Before the onset of CSD, even though all the samples are under different stress states and densities, all have become unstable during CSD loading. In this study, the decrease of deviatoric stress was also captured by the ratio of incremental stress ratio dq/dp', where an abrupt rise in the incremental stress ratio was noticed at the onset of instability. In addition, the DEM model has captured the dilation behaviour of axial strain after the onset of CSD condition at higher confining stresses. The stress ratio at the onset of CSD condition has shown influence on the evolution of micro-mechanical quantities, a_n and a_c. The rate of increase in a_c varied after imposing CSD condition and its growth continued beyond the instability due to the rearrangement of contacts in the loading direction. Whereas, the response of a_n changed from linear to nonlinear increments after imposing CSD loading and after the instability point a_n decreased indicating the lack of ability to withstand the load while p' is decreasing. Overall, the DEM model successfully predicted the instability point similar to the experimental data and qualitatively captured the macroscopic response.

Acknowledgement

The authors acknowledge the assistance of all university partners (University of Western Australia (lead university), University of New South Wales, University of South Australia, and University of Wollongong) involved in this project. This work is part of TAILLIQ (Tailings

Liquefaction) project, which is an Australian Research Council (ARC) Linkage Project supported by Anglo American, BHP, Freeport-McMoRan, Newmont, Rio Tinto, and Teck.

References

Alipour MJ, Lashkari A (2017) Prediction of Sand Instability Under Constant Shear Drained Paths. Paper presented at the Bifurcation and Degradation of Geomaterials with Engineering Applications, Cham.

Anderson Scott A, Riemer Michael F (1995) Collapse of Saturated Soil Due to Reduction in Confinement. Journal of Geotechnical Engineering, 121(2), 216-220. doi:10.1061/(ASCE)0733-9410(1995)121:2(216)

Bagi K (1996) Stress and strain in granular assemblies. Mechanics of Materials, 22(3), 165-177. doi:https://doi.org/10.1016/0167-6636(95)00044-5

Brand EW (1981) Some thoughts on rain-induced slope failures. Proc. 10th ICSMFE, 1981, 3, 373-376.

Chu J, Leong WK, Loke WL, Wanatowski D (2012) Instability of Loose Sand under Drained Conditions. Journal of Geotechnical and Geoenvironmental Engineering, 138(2), 207-216. doi:10.1061/(ASCE)GT.1943-5606.0000574

Chu J, Leroueil S, Leong WK (2003) Unstable behaviour of sand and its implication for slope instability. Canadian Geotechnical Journal, 40(5), 873-885. doi:10.1139/t03-039

Cui L, O'Sullivan C (2006) Exploring the macro- and micro-scale response of an idealised granular material in the direct shear apparatus. Géotechnique, 56, 455-468. doi:10.1680/geot.56.7.455

Cundall PA, Strack ODL (1979) A discrete numerical model for granular assemblies. Géotechnique, 29(1), 47-65. doi:10.1680/geot.1979.29.1.47

Daouadji A, AlGali H, Darve F, Zeghloul A (2010) Instability in Granular Materials: Experimental Evidence of Diffuse Mode of Failure for Loose Sands. Journal of Engineering Mechanics, 136(5), 575-588. doi:10.1061/(ASCE)EM.1943-7889.0000101

Darve F, Servant G, Laouafa F, Khoa HDV (2004) Failure in geomaterials: continuous and discrete analyses. Computer Methods in Applied Mechanics and Engineering, 193(27), 3057-3085. doi:https://doi.org/10.1016/j.cma.2003.11.011

Darve F, Sibille L, Daouadji A, Nicot F (2007) Bifurcations in granular media: macro- and micro-mechanics approaches. Comptes Rendus Mécanique, 335(9), 496-515. doi:https://doi.org/10.1016/j.crme.2007.08.005

Dong Q, Xu C, Cai Y, Juang H, Wang J, Yang Z, Gu C (2016) Drained Instability in Loose Granular Material. International Journal of Geomechanics, 16(2), 04015043. doi:10.1061/(ASCE)GM.1943-5622.0000524

Eckersley D (1990) Instrumented laboratory flowslides. Géotechnique, 40(3), 489-502. doi:10.1680/geot.1990.40.3.489

Fu P, Dafalias YF (2011) Study of anisotropic shear strength of granular materials using DEM simulation. International Journal for Numerical and Analytical Methods in Geomechanics, 35(10), 1098-1126. doi:10.1002/nag.945

Gajo A, Piffer L, De Polo F (2000) Analysis of certain factors affecting the unstable behaviour of saturated loose sand. Mechanics of Cohesive-frictional Materials, 5(3), 215-237. doi:10.1002/(SICI)1099-1484(200004)5:3<215::AID-CFM92>3.0.CO;2-7

Guo N, Zhao J (2013) The signature of shear-induced anisotropy in granular media. Computers and Geotechnics, 47, 1-15. doi:https://doi.org/10.1016/j.compgeo.2012.07.002

Hadda N, Nicot F, Bourrier F, Sibille L, Radjai F (2013) Micromechanical Analysis of Second Order Work in Granular Media. Granular Matter, 15. doi:10.1007/s10035-013-0402-3

Head KH, Epps R. (2011). Manual of Soil Laboratory Testing: Whittles Publishing.

Hill R (1958) A general theory of uniqueness and stability in elastic-plastic solids. Journal of the Mechanics and Physics of Solids, 6(3), 236-249. doi:https://doi.org/10.1016/0022-5096(58)90029-2

Huang X, Hanley KJ, O'Sullivan C, Kwok FCY (2014) Effect of sample size on the response of DEM samples with a realistic grading. Particuology, 15, 107-115. doi:https://doi.org/10.1016/j.partic.2013.07.006

Itasca (2016). Particle flow code in 3D version 5 software manual. Minnesota, MN, USA

Iwashita K, Oda M. (1999). Mechanics of Granular Materials: An Introduction: Taylor & Francis.

Lashkari A, Khodadadi M, Binesh Seyed M, Rahman Md M (2019) Instability of Particulate Assemblies under Constant Shear Drained Stress Path: DEM Approach. International Journal of Geomechanics, 19(6), 04019049. doi:10.1061/(ASCE)GM.1943-5622.0001407

Marketos G, Bolton MD (2010) Flat boundaries and their effect on sand testing. International Journal for Numerical and Analytical Methods in Geomechanics, 34(8), 821-837. doi:10.1002/nag.835

MiDi GDR (2004) On dense granular flows. The European Physical Journal E, 14(4), 341-365. doi:10.1140/epje/i2003-10153-0

Nicot F, Daouadji A, Laouafa F, Darve F (2011) Second-order work, kinetic energy and diffuse failure in granular materials. Granular Matter, 13(1), 19-28. doi:10.1007/s10035-010-0219-2

Nicot F, Hadda N, Bourrier F, Sibille L, Wan R, Darve F (2012) Inertia effects as a possible missing link between micro and macro second-order work in granular media. International Journal of Solids and Structures, 49(10), 1252-1258. doi:https://doi.org/10.1016/j.ijsolstr.2012.02.005

Ning Z, Evans TM, Andrade J (2013) Particulate Study of Drained Diffuse Instability in Granular Material.

Olson S, Stark T, Walton W, Castro G (2000) 1907 Static Liquefaction Flow Failure of the North Dike of Wachusett Dam. Journal of Geotechnical and Geoenvironmental Engineering - J GEOTECH GEOENVIRON ENG, 126. doi:10.1061/(ASCE)1090-0241(2000)126:12(1184)

O'Sullivan C. (2011). Particulate Discrete Element Modelling: A Geomechanics Perspective: CRC Press.

Perez JCL, Kwok CY, O'Sullivan C, Huang X, Hanley KJ (2016) Exploring the micro-mechanics of triaxial instability in granular materials. Géotechnique, 66(9), 725-740. doi:10.1680/jgeot.15.P.206

Rabbi Abu Taher Md Z, Rahman Md M, Cameron D (2019) Critical State Study of Natural Silty Sand Instability under Undrained and Constant Shear Drained Path. International Journal of Geomechanics, 19(8), 04019083. doi:10.1061/(ASCE)GM.1943-5622.0001462

Ramos AM, Andrade JE, Lizcano A (2012) Modelling diffuse instabilities in sands under drained conditions. Géotechnique, 62(6), 471-478. doi:10.1680/geot.10.P.109

Reid D, Fourie A (2019) A direct simple shear device for static liquefaction triggering under constant shear drained loading. Géotechnique Letters, 9(2), 142-146. doi:10.1680/jgele.19.00011

Rothenburg L, Bathurst RJ (1989) Analytical study of induced anisotropy in idealized granular materials. Géotechnique, 39(4), 601-614. doi:10.1680/geot.1989.39.4.601

Sasitharan S, Robertson P, Sego D, Morgenstern N (1993) Collapse behavior of sand. Canadian Geotechnical Journal - CAN GEOTECH J, 30, 569-577. doi:10.1139/t93-049

Satake M (1982) Fabric tensor in granular materials. In Deformation and failure of granular materials (eds P. A. Vermeer and H. J. Luger), 63–68. Rotterdam, the Netherlands: Balkema.

Sawicki A, Świdziński W (2010) Modelling the pre-failure instabilities of sand. Computers and Geotechnics, 37(6), 781-788. doi:https://doi.org/10.1016/j.compgeo.2010.06.004

Sibille L, Nicot F, Donzé FV, Darve F (2007) Material instability in granular assemblies from fundamentally different models. International Journal for Numerical and Analytical Methods in Geomechanics, 31(3), 457-481. doi:10.1002/nag.591

Sitharam TG, Vinod JS (2010) Evaluation of Shear Modulus and Damping Ratio of Granular Materials Using Discrete Element Approach. Geotechnical and Geological Engineering, 28(5), 591-601. doi:10.1007/s10706-010-9317-5

Sitharam TG, Vinod JS, Ravishankar BV (2008) Evaluation of undrained response from drained triaxial shear tests: DEM simulations and experiments. Géotechnique, 58(7), 605-608. doi:10.1680/geot.2008.58.7.605

Skopek P, Morgenstern NR, Robertson P, Sego D (2011) Collapse of dry sand. Canadian Geotechnical Journal, 31, 1008-1014. doi:10.1139/t94-115

Zhu J-H, Anderson SA (1998) Determination of shear strength of Hawaiian residual soil subjected to rainfall-induced landslides. Géotechnique, 48(1), 73-82. doi:10.1680/geot.1998.48.1.73

List of Figures

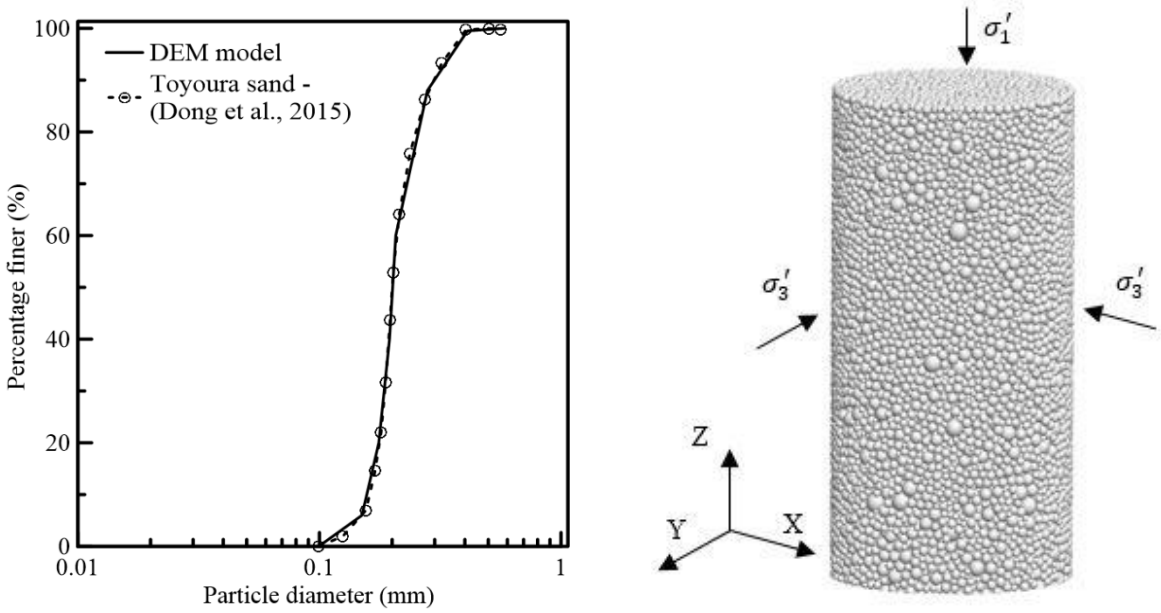

(a) (b)

Figure 1. (a): Particle size distribution curve of DEM simulations. (b): The representative element volume of DEM sample.

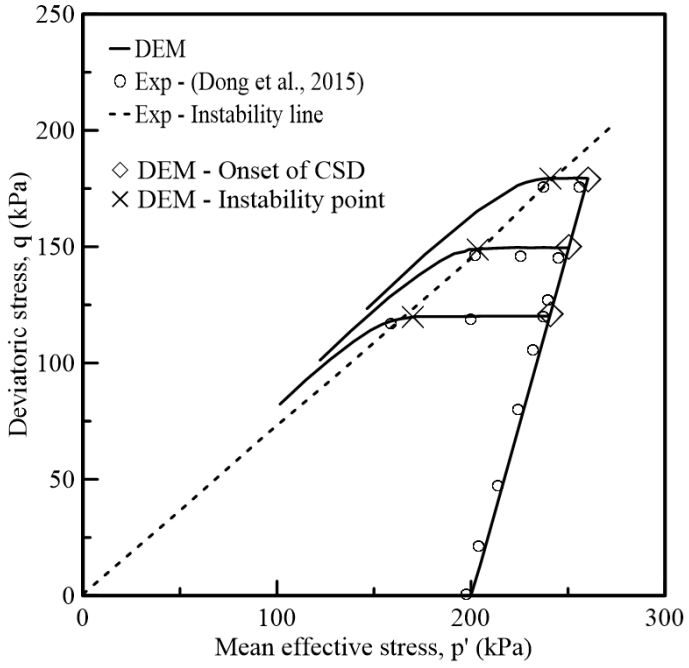

Figure 2. Deviatoric Stress versus Mean effective stress during CSD Simulation along with experimental results of Dong et al. (2015).

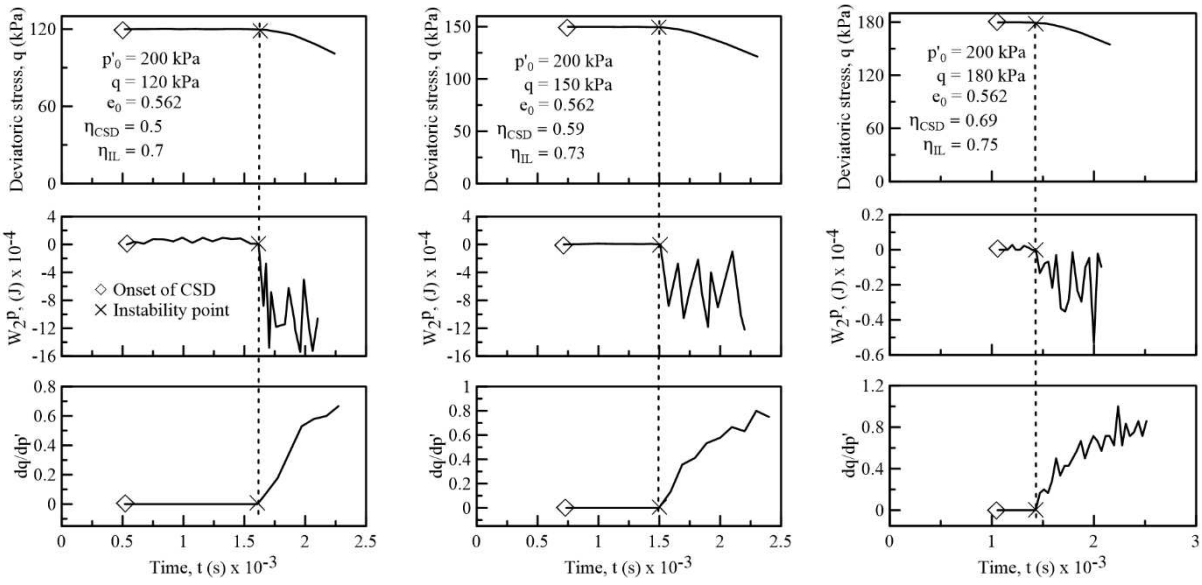

(a) (b) (c)

Figure 3(a), (b), (c). Variation of deviatoric stress, particle scale second order work, gradient dq/dp' against time.

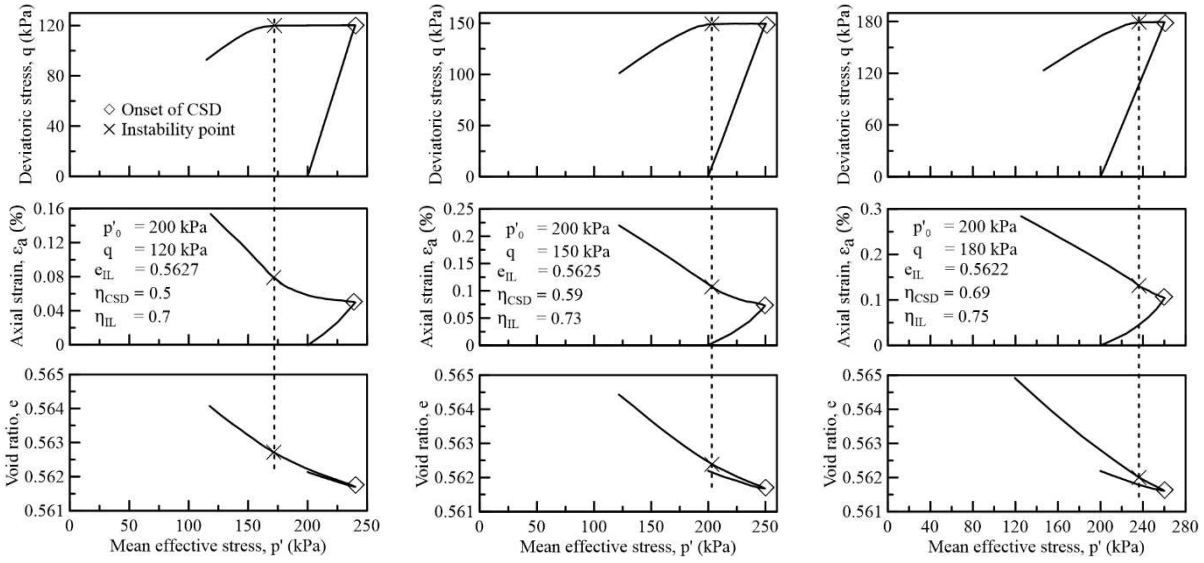

(a) (b) (c)

Figure 4(a), (b), (c). Deviatoric stress, axial strain, void ratio versus Mean effective stress.

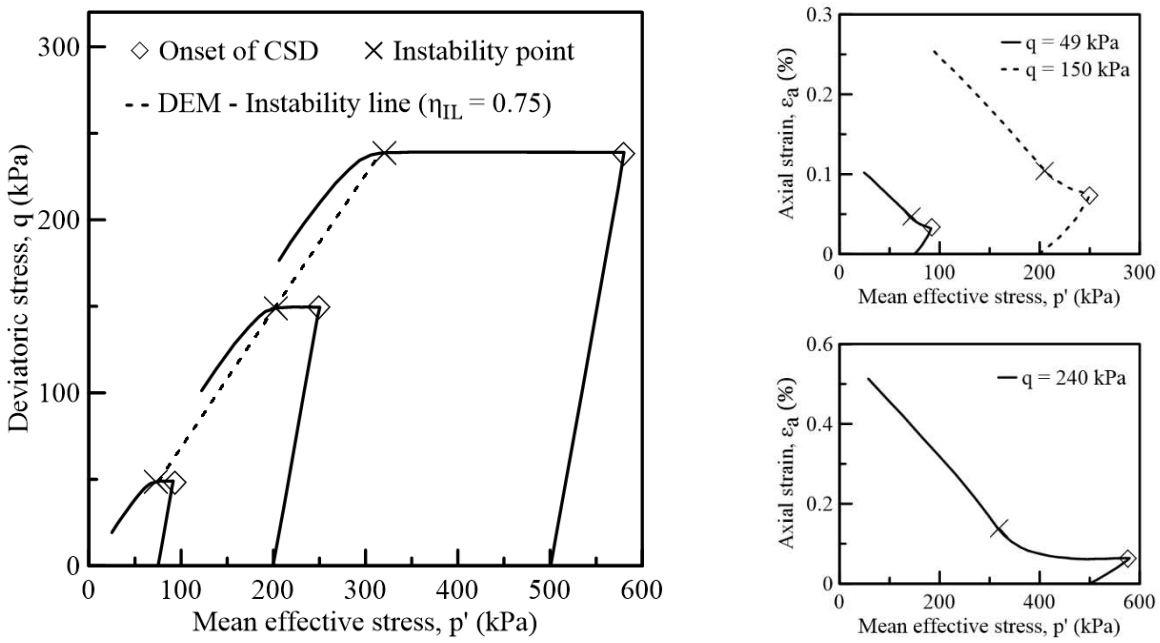

(a) (b)

Figure 5. (a): Comparison of CSD tests response for p′= 75, 200, 500 kPa. (b): Variation of axial strain against mean effective stress: Effect of p′.

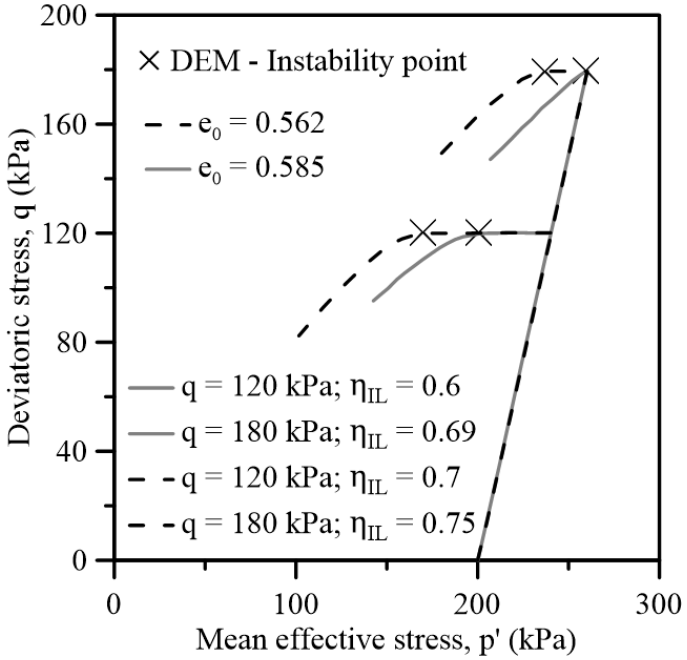

Figure 6. Deviatoric Stress versus Mean effective stress: Effect of void ratio.

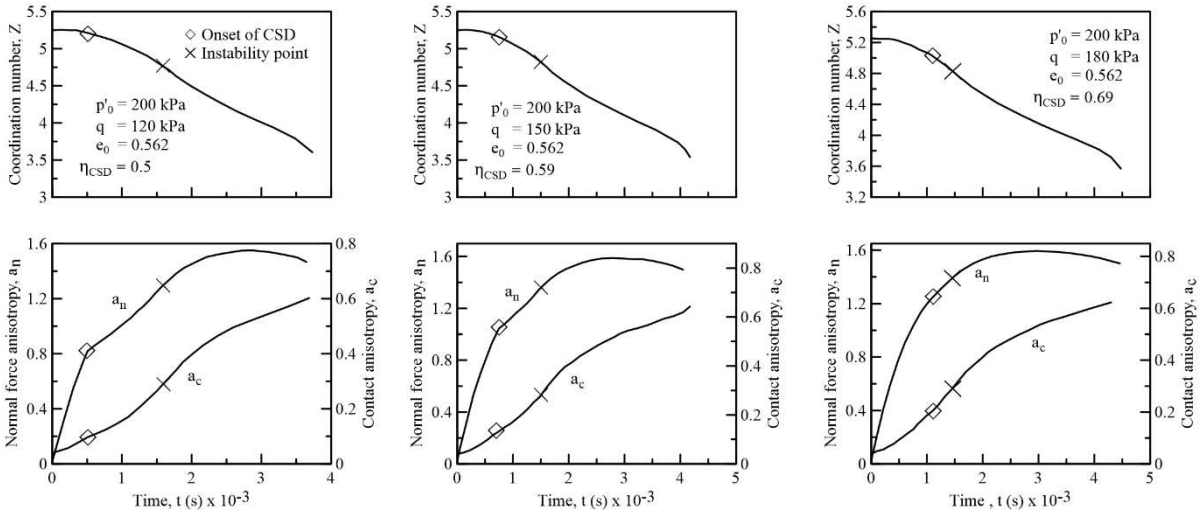

(a) (b) (c)

Figure 7(a), (b), (c). Variation of coordination number, normal force anisotropy and contact anisotropy against time for all three stress states.

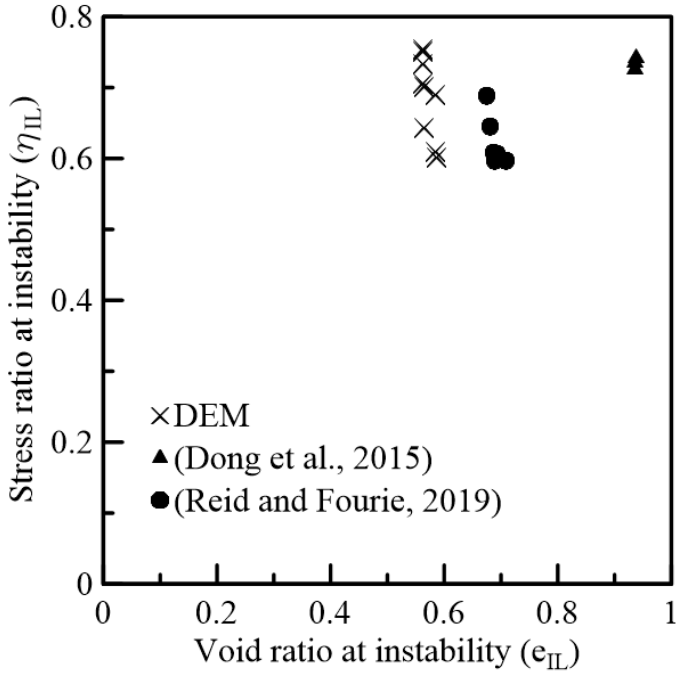

Figure 8. Stress ratio against void ratio at instability.